

# Influence of Building Geometry on Wind Power Potential

Mikhail Yakhnis<sup>1</sup>, Rogerio Bonatti<sup>2</sup>, Ryan Gryszko<sup>3</sup>, Chinazo Obiejesi<sup>4</sup>  
Cornell University, Ithaca, NY, 14853

Wind flow behavior is influenced by obstacles in the environment. Altering the geometry of buildings yields certain flow characteristics that are important in evaluating the performance of wind energy harvesting systems mounted on a structure. By varying the angle of a building's façade relative to the horizontal, we are able to accelerate the flow and maximize the available wind power for wind energy harvesting. Wind tunnel testing was done in a simulated boundary layer with both a basic rectangular model and a 30 degree sloped model. Utilizing hot wire anemometry, data was gathered along the center-line of each model. It was found that there was a velocity increase between 16% and 35% at the sloped model's rooftop leading edge resulting in an increase in power production between 56% and 150%. The region of interest corresponds to an area no more than one and a half inches of height above the model, equating to twenty-five feet in real-world height using our scale factor of 1:200. Additionally, the turbulence intensity was negligibly affected by the sloped model. We conclude that altering the geometry of buildings in this manner can be extremely beneficial to energy production using small wind turbines at the leading edge of structures.

## Nomenclature

$\rho$	=	air density ( $\text{kg m}^{-3}$ )
$A$	=	swept area of turbine ( $\text{m}^2$ )
$U_0$	=	free-stream air velocity ( $\text{m s}^{-1}$ )
$\alpha$	=	model's front slope
$T_r$	=	turbulence intensity
$P_0$	=	available power density
$P_T$	=	power generated by turbine
$C_p$	=	coefficient of performance
$F_r$	=	wind tunnel's motor frequency of rotation

## I. Introduction

In 2011, buildings used over 60% of electricity generated and accounted for almost 40% of overall energy use in the United States<sup>6</sup>. Due to increasing concerns over sustainability, climate change, and energy independence, a number of renewable energy options have been explored in recent years. Wind power in particular has grown rapidly, with generated power increasing 84% from 2009 to 2012 to compose 3.5% of total generated electricity.<sup>2</sup> However, most of this increased generation has come from utility scale wind farms which suffer from one of the disadvantages common to any utility scale energy generation site, namely transmission losses exacerbated by remote siting.

A potential solution to this issue lies in microscale wind power devices such as VAWTs (Vertical Axis Wind Turbines) or the Crossflex system<sup>1</sup>. These turbines allow for localized energy collection in areas otherwise unfeasible for traditional HAWTs (Horizontal Access Wind Turbines) such as the built environment. Heath<sup>3</sup> estimated that annual yield from a small-scale turbine mounted on the roof of a ten meter high residence could be on the order of 500 kWh. Although Heath's experiment used empirical data in order to perform the CFD (Computational Fluid Dynamics) analysis of such a residence, Heath admitted that there was a lack of data on the flow conditions around buildings. Sharpe<sup>1</sup> corroborates this lack of data and adds that existing buildings, which often have poor energy efficiency, could see the most benefit from integrated energy generation modules.

As such, a number of wind-tunnel experiments using HWA (hot-wire anemometry) and simulations were designed to elucidate the flow characteristics around bluff bodies in urban and suburban environments. The goal was

---

<sup>1</sup> Student Researcher, Mechanical Engineering, 13300 W. 105<sup>th</sup> St, Lenexa, KS, 66215, USA. Student Member.

<sup>2</sup> Student Researcher, Mechanical Engineering, R. Madre Mazarello, 199, São Paulo SP, 05454-040 Brazil. Student Member.

<sup>3</sup> Student Researcher, Mechanical Engineering, 56 Garden Street, Little Ferry, New Jersey 07643, USA. Student Member.

<sup>4</sup> Student Researcher, Mechanical Engineering, 226 Upson Hall, Cornell University, Ithaca, NY 14850. Student Member.

firstly to determine, given a particular building geometry, the optimal placement of a micro-scale wind power device. Broadly, this location would have two critical characteristics: high velocity as compared to the oncoming flow and comparatively low turbulence. The latter point is of particular importance as Glass<sup>4</sup>, relating the findings of the WINEUR project, found that turbulence in the built environment reduced turbine output by 15-30%. On the other hand, it has also been documented by Dannecker<sup>5</sup> that bluff bodies do in fact increase the velocity, especially around the leading edge of a structure.

Once the experimental setup had been calibrated and was yielding similar results to the CFD for more simple test cases, the empirical results and simulation data were used in conjunction so that the authors could come as close as possible to the actual flow conditions occurring in the tunnel. Limiting these efforts was the ability to only measure the magnitude of the velocity in a given plane (due to the use of a “U-wire” anemometry probe). Also, vibrations present in the experimental assembly complicated efforts to measure turbulence intensity.

Three main results were obtained for models of various geometries: velocity, turbulence intensity, and available wind power as a percentage of free stream wind power.

Once the optimization of high velocity and low turbulence had been found, the authors explored how to optimize building geometry in order to facilitate energy harvesting. This optimization could lead to true building-integrated solutions.

## II. Wind Turbine and Atmospheric Boundary Layer Theory

Considering a unidirectional flow of air in space going through an area  $A$ , the total power available in the wind is a function of its kinetic speed<sup>7</sup>, and is given by Equation (1):

$$P_0 = \frac{1}{2} * \rho * A * U_0^3 \quad (1)$$

It is important to note that the power present in the wind differs from the total power that can be extracted by a real rotor by a factor of  $C_p$ , which is limited by the *Betz Limit* value of 0.59, and is related to the physical characteristics of the turbine. A simple analysis of equation (1) shows that by increasing the incoming speed by a factor  $f_{inc}$ , the resulting power captured by the turbine will be increased by  $(f_{inc})$  cubed (assuming that  $C_p$  remains constant, what generally occurs in practice), which demonstrates the importance of finding sites where the wind velocity is greater than the mean incoming speed to place the turbines.

The incoming flow is not uniform in space or time, and is highly dependent on the height relative to the ground and on the terrain's roughness (Fig. 1). The flow's mean velocity varies differently depending on the type of terrain<sup>8</sup>, as postulated by Mertens<sup>8</sup> in equations (2), for an approximately flat terrain and (3), for an urban environment:

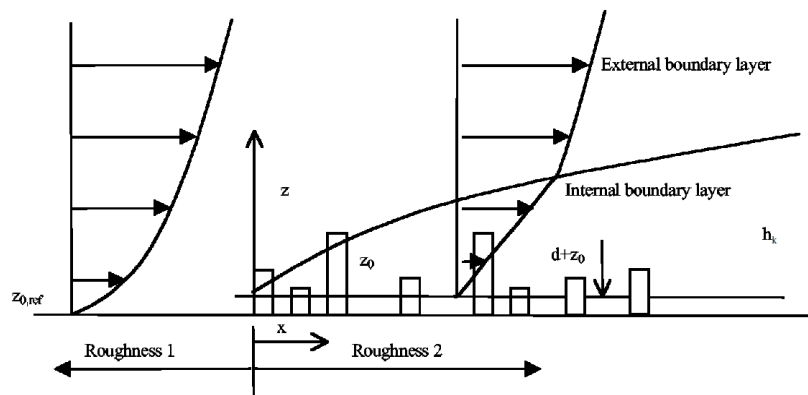


**Figure 1. Sketch of boundary layer across different terrain types.** *The behavior of the flow is different in the atmospheric boundary layer found in a relatively flat terrain and in an urban environment. Figure adapted from Mertens<sup>8</sup>.*

$$U(z) = \frac{U^*}{k} * \ln \left( \frac{z}{z_0} \right) \quad (2)$$

$$u_0(z) = \frac{\ln \left( \frac{h_k(x)}{z_{0 \text{ ref}}} \right) * \ln \left( \frac{z-d}{z_0} \right)}{\ln \left( \frac{h_{\text{ref}}}{z_{0 \text{ ref}}} \right) * \ln \left( \frac{h_k(x)-d}{z_0} \right)} * u_{\text{ref}} \quad (3)$$

where  $U^*$  is the friction velocity,  $k$  is the Von Karman constant (0.4),  $z_0$  is the surface roughness length,  $h_k$  is the internal boundary layer's height,  $d$  is the displacement length, and the indexes denoted with  $ref$  are referent to the values for the undisturbed wind, found in a wind atlas.

**Experiments in the wind tunnel and the computational simulations were performed using a determined surface roughness length, in order to emulate the physical phenomena as close as possible to reality.**

### III. Preparation of Wind Tunnel Experiments and Boundary Layer CFD Analysis

#### A. Wind Tunnel and Models Dimensions and Scaling Factor

Testing was done in a 1m wide by 0.9m high by 20m long test section. To help ensure accurate results for all model types (both 2D and 3D), we made sure that there was no more than 15% blockage in the cross section of the tunnel.<sup>10</sup> From this consideration, the models were scaled to a 1:200 ratio.

Taking the maximum tunnel blockage ratio into account, the models were designed with a constant height of 0.3m. We created 4 models (Fig. 2), referent to 3 different situations:

- a) 3D flow around a rectangular block (0.1m of width and 0.1m length)
- b) 2D flow around a rectangular block (0.5m width and 0.1m length)
- c) 2D & 3D flow around a sloped block (slope  $\alpha = 30^\circ$ )

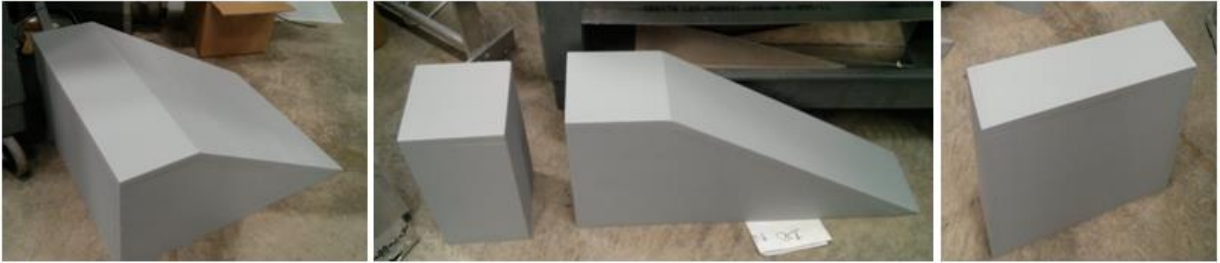


**Figure 2. Physical models used for the wind tunnel experiments.** All models have a height of 0.3m, and width of 0.1m (simulation of 3D flow around building) or 0.5m (simulation of 2D flow). One model has a sloped façade of  $30^\circ$ .

#### B. 2D Testing of Boundary Layer Growth

To determine the best approach for growing our boundary layer, the team created multiple CFD simulations to estimate which case best creates the boundary layer effect we seek. These simulations were based on the use of spires and roughness elements<sup>9</sup>. In our simulations, the roughness elements represent the earth's roughness length of roughly 2 meters, and the spires are used to generate turbulence and thicken the boundary layer. The three simulations and the resulting plots are shown in Fig. 3:

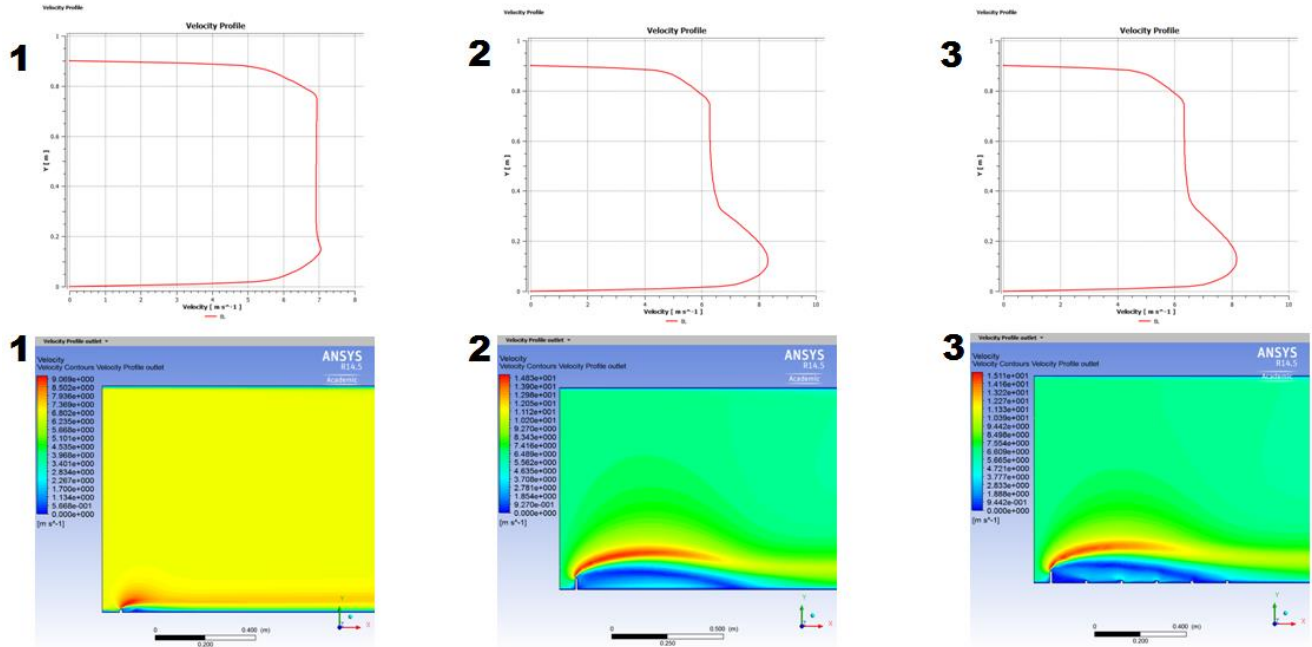


**Figure 3.** 2D CFD simulations of different roughness elements and spires. The three simulations were performed using different spires and roughness elements configurations.

By inspecting Simulation 1 in Figure 3, we see that although the roughness elements do contribute to some boundary layer growth, they are not substantial enough on their own to develop an atmospheric boundary layer that is thicker than a building's height. In simulation 2, without the roughness elements, we note that the boundary layer presents an increase in height as desired, but we see that the roughness elements contribute to a quicker development of the profile. In the third simulation, however, one can notice that with a bigger spire and with the addition of roughness elements the boundary layer grows to the desired height and develops quickly.

By analyzing the results obtained in the simulations, we can see that the appropriate model consists of tall spires at the entrance of air followed by a set of smaller roughness elements (essentially square blocks). The spires are designed with utilizing Irwin's equations<sup>9</sup> (Eq. 4 to 8), using the following set of variables: height of the tunnel,  $H$ , is 0.95m and we are looking for a boundary layer,  $\delta$ , of at least 0.5m. To achieve this result we utilized a constant coefficient,  $\alpha$ , of 0.4. These equations yield the heights of the spires,  $h$ , of 0.5792m and their widths,  $b$ , of 0.1131m:

$$H = .95 \text{ m} \quad \alpha = .4 \quad \delta = .5 \text{ m}; \quad (4) \quad B = \left(\frac{\delta}{H}\right)\left(\frac{\alpha}{1+\alpha}\right) \quad (5)$$

$$\Psi = \frac{B \left( \frac{2}{1+2\alpha} + B - \left( \frac{1.13\alpha}{1+\alpha} \right) \right)}{(1-B)^2} \quad (6) \quad h = \frac{1.39\delta}{1+\frac{\alpha}{2}} \quad (7)$$

$$b = \frac{h}{2} \left( \frac{\Psi H}{1+\Psi} \right) \left( 1 + \frac{\alpha}{2} \right) \quad (8)$$

Regarding the sizing of the roughness elements, Garthshore<sup>11</sup> referred to different methods of determining the dimensions but all were based on scaling down earth's roughness of at most 7 meters. The paper also suggests an agreement on the alignment of the elements in rows and columns of a pre-determined fetch depending on the number of roughness elements incorporated into the design, being placed along the tunnel's flow in a 15% plane density.

### C. 3D Testing of Boundary Layer Growth

The spires and roughness elements were designed with the aid of a CAD tool (SolidWorks, Dassault Systèmes, France) and before being machined, several configurations of roughness elements and spires were generated from the ideal 2D models to be tested now in 3D CFD simulations. The results of the simulations can be found below (Fig. 4):

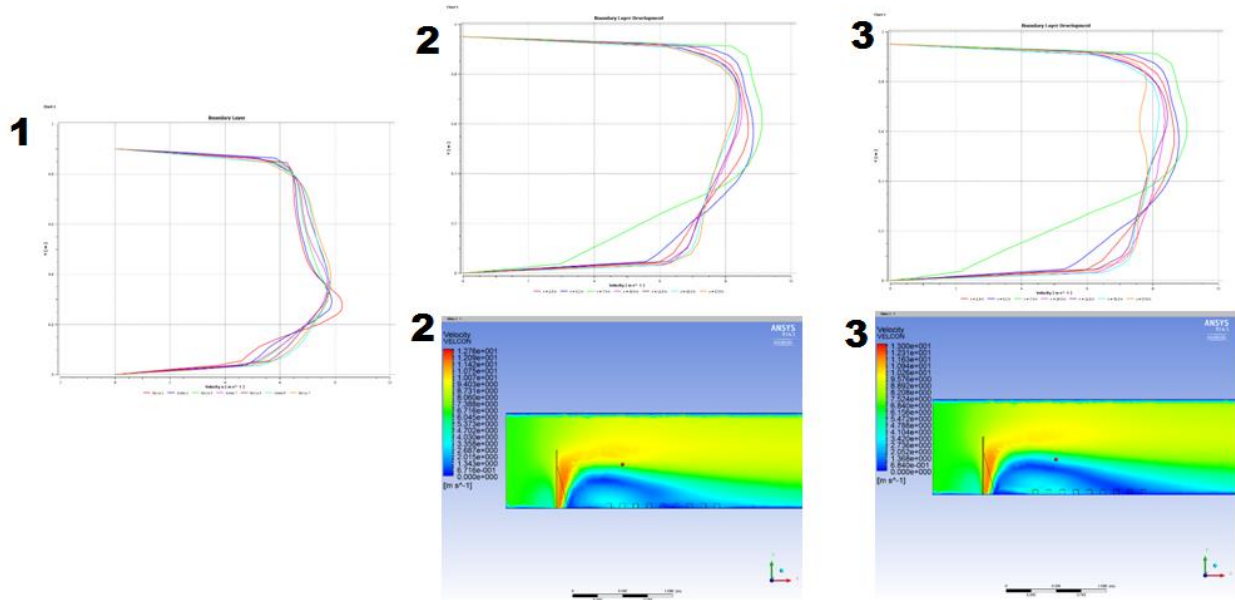


**Figure 4.** 3D CFD simulations of different roughness elements and spires. The three simulations were performed using different spires and roughness elements configurations.

Difficulties were found in making the 3D CFD simulations converge, and after troubleshooting, we found that the issues resided in the way the geometry was being meshed and the model being used to solve the Navier-Stokes equations. The best solution that converged was a K-Epsilon ( $k-\epsilon$ ) model with enhanced wall treatment for a coarse mesh with body sizing close to the roughness elements. K-Omega ( $k-\omega$ ) is the model of choice for 3D simulations but without a reasonable guess for these parameter values via the actual experiment, the simulation can only use estimates of the results.

Although the first simulation depicted in Fig. 4 was created without the addition of the splitter plate (element used to divert the turbulent flow generated by the spires) in the spires and with roughness elements of height 0.01m, it served as a starting point for the group to physically understand the outcome of future simulations. A stabilization of the boundary layer was achieved 10m after the tunnel's entrance, and its height was 0.4m, taller than the model as desired. Better results were achieved in simulations 2 and 3, where the height of the roughness elements was 0.05m and 0.1m respectively. It was found that the height of the boundary layer was directly proportional to the height of the blocks. In evaluating other parameters, we found that there was no correspondence between the density of blocks (altered by the adjustment of parameters  $x$ ,  $y$  and  $z$  in Fig. 5), and the height of the boundary layer.

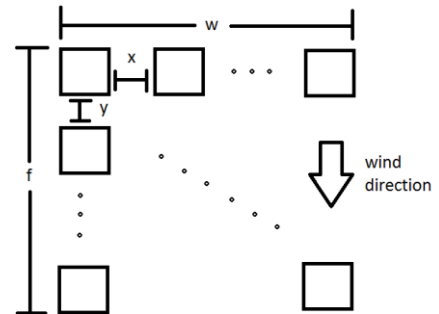


**Figure 5.** Top view of placement of roughness elements at the wind tunnel

### D. Construction and assembly of spires and roughness elements

After gathering information related to the boundary layer elements optimization, together with equations set (4) to (8), the spires were designed to be isosceles triangles with a base and height of 0.1131m and 0.5792m respectively, held together by a splitter plate which is a right triangle with height of 0.42m and base angle of  $75^\circ$  (Fig. 4), while the roughness elements were designed as wooden cubes (0.05m edge). The cubes were epoxied on a 1/16" aluminum plate, following the scheme of Fig. 5, where  $f$  is the fetch of the roughness elements which is 113

cm,  $w$  is the width which is 80 cm,  $x$  is the horizontal separation which is 10 cm and  $y$  is the vertical separation which is 8.5 cm (Fig. 6).

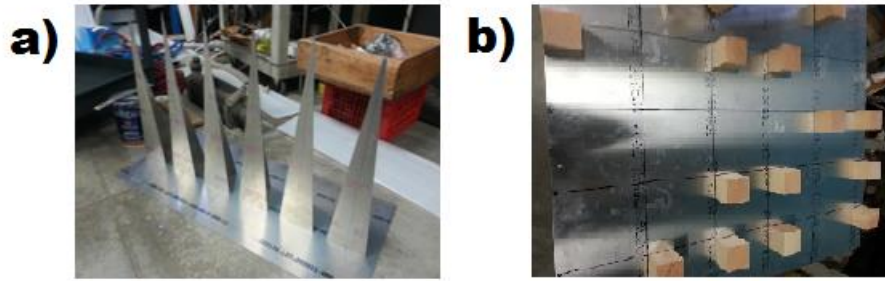


**Figure 6. Photographs of elements used to simulate the atmospheric boundary layer in wind tunnel experiments. a) Spires and b) Square roughness elements.**

#### IV. Wind Tunnel Models' CFD Analysis

After determining the velocity profile resulting from the addition of the spires and roughness elements, CFD simulations were done to determine the theoretical velocity contours for real-sized buildings on which our models were based on. These results are shown in Figure 7. These simulations are to be used as a theoretical comparison for the results obtained with the actual wind tunnel experiment, to quantify how well the experiment matches the behavior of the air flowing around a real building.

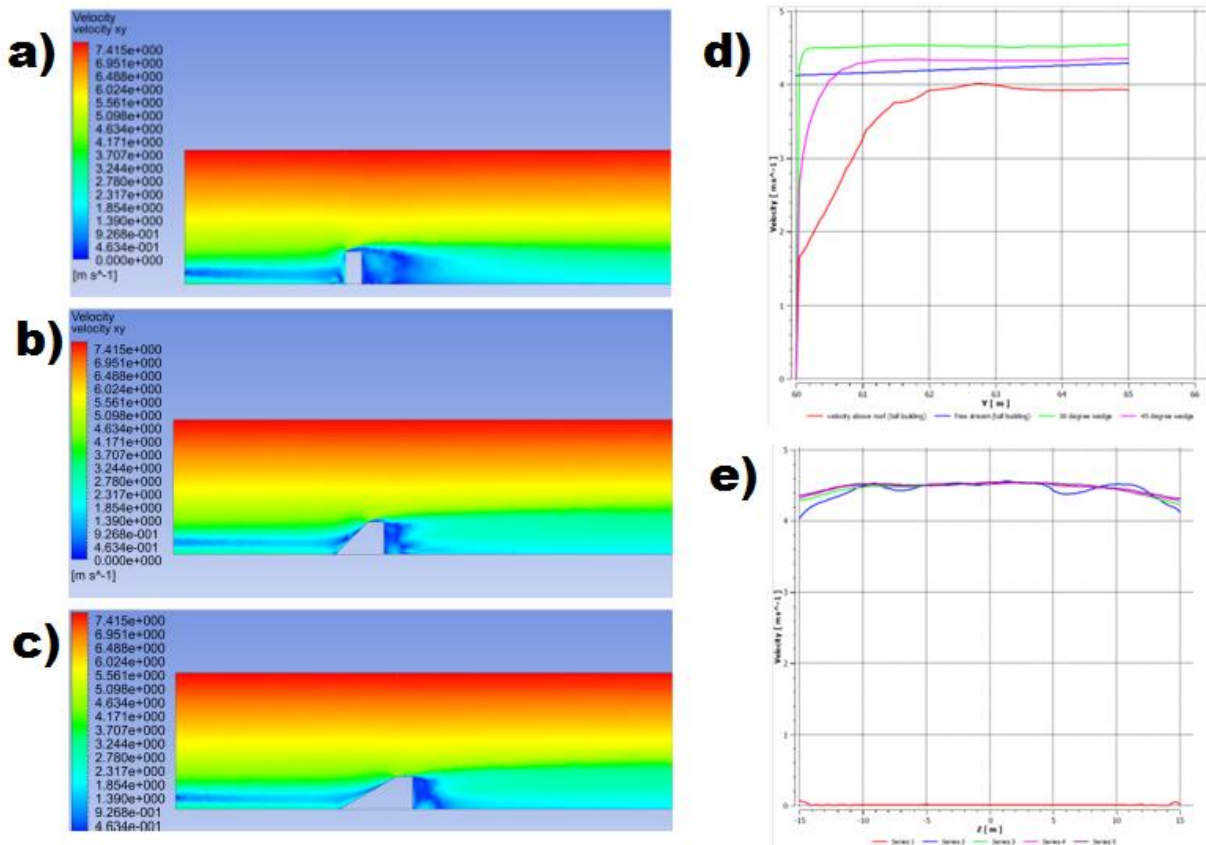


**Figure 7. CFD simulations of air flow around real-sized buildings. a) 2D airflow around rectangular building; b) 2D flow around 45° sloped building; c) 2D flow around 30° slope; d) Velocity data taken from buildings a, b and c (red, green and magenta, respectively) and compared to the free stream velocity (blue) at the leading edge, from 0m to 5m of height; e) Using a front view at a 3D flow around the rectangular building, velocity was**

*captured at heights of 1,2,3,4 and 5m from the rooftop, 15m from the middle of the leading edge to the right and to the left, to detect the effect of the vortices at the edges of the building.*

## V. Wind Tunnel Experiments

### A. Wind tunnel's characteristics and robotic XYZ platform for data capturing

The wind tunnel used for experiments has a length of 20m and a rectangular cross section of 0.95m in height and 1.0m in width. The maximum speed is 17m/s, and the speed is controlled by adjusting a turbine's rotational frequency from 0Hz to 50Hz. It is a suction tunnel, where the turbine is placed at one extremity of the tunnel and blows air out of the section, causing a drop in pressure inside the tunnel and allowing the air to be sucked at the opposing extremity. The inlet is protected by several layers of screens and by vertically positioned metal plates to protect the experiment from external debris and to diminish turbulent effects at the entrance of the tunnel. All experiments are run at a distance of 15 meters from the entrance, where a stable boundary layer has already been developed.

A robotic platform is used to hold a hot wire anemometer to measure the wind speed at various points in space. This platform has stepper motors in the XYZ directions, and is controlled by an Atmega 1284 microcontroller integrated to a LabVIEW PXI computer to capture the data and move the anemometer through space. Dampers were strategically placed in the Z axis to prevent vibrations caused by vortex shedding from the edges of the Z column, and vibrations caused at the anemometer support, which can influence the measurement of turbulence and mean velocity in the flow.

### B. Hot wire anemometer theory and calibration curves

A hot wire anemometer is a thin wire that is heated to a certain temperature (in our case around 250°C) and exposed to an air flow. There are different types of hot wire anemometers; we use a Constant Temperature Anemometer (CTA). The anemometer is connected to a transducer (DISA 55M Bridge, IBM) that supplies the wire with an electrical current. By the Joule effect, the anemometer heats up (due to the resistivity of the wire), and if an air flow is present, a higher voltage must be applied to the terminals of the anemometer to maintain the same temperature (due to convective heat loss to the flow). We measure the output voltage of the transducer, and the higher the flow speed, the higher the voltage outputted by the device.

Theoretically, this voltage increase follows King's Law<sup>8</sup> (Eq. 9, achieved taking into account the fluid mechanics and thermodynamics in the flow around the wire), where  $n$  varies from 0.45 to 0.5 and  $A$  and  $B$  are the calibration coefficients that must be experimentally determined:

$$E^2 = A + Bu^n \quad (9)$$

During the actual testing, the hot wire is used in vertical and horizontal configurations, so we calibrated the hot wire in both positions. We have access to a digital hot wire anemometer that we fixed in one point in space inside the tunnel, and we changed the tunnel's velocity by stepping through turbine frequency in 5Hz increments from 0Hz to 50Hz. For each frequency (each velocity), we wrote down the 1 minute average of the velocity shown by the digital anemometer in that point in space.

We then removed the digital anemometer and inserted the hot wire anemometer into the tunnel, in the same point in space where the digital anemometer was, and we turned on the tunnel at the exact same frequencies as before. For each new frequency, we waited about 5 minutes until the tunnel was again stable and we then took 60 seconds of the output voltage data at a sampling frequency of 10kHz.

Next, we averaged the 60 seconds of data to obtain one average velocity value at that point in space, and then we fitted a curve to the experimental points to find the Kings Law's coefficients  $A$  and  $B$ . This was done twice, yielding the following two calibration equations (for vertical and horizontal configurations, Eq. 10):

$$\text{Horizontal: } V^2 = 9.444U^{0.45} + 13.48 \quad \text{Vertical: } V^2 = 9.661U^{0.45} + 13.12 \quad (10)$$

### C. Wind Tunnel's Characterization

Before testing around the models, it was necessary to characterize the tunnel to assess the validity of our experimental data by comparing it to CFD. Before installing the roughness elements and spires, we measured a velocity profile of just the tunnel itself. To do this we performed tests with the hot wire anemometer in the vertical

configuration for the first eight inches and then in the horizontal configuration for the remaining points we were able to reach. Then, we installed the roughness elements to understand their effect on the boundary layer development and took another profile in the same fashion as the first. Lastly, we installed our main flow tripping device, the spires, and performed another characterization of the tunnel. Figure 8 shows the three profiles overlaid on the same graph. All of the characterizations were performed at a controller setting of 25 Hz. After observing all the profiles, we decided to increase the speed for the test around the model to 30 Hz to yield the proper flow characteristics. We did this with the intention to later go back and recharacterize the tunnel at 30Hz.

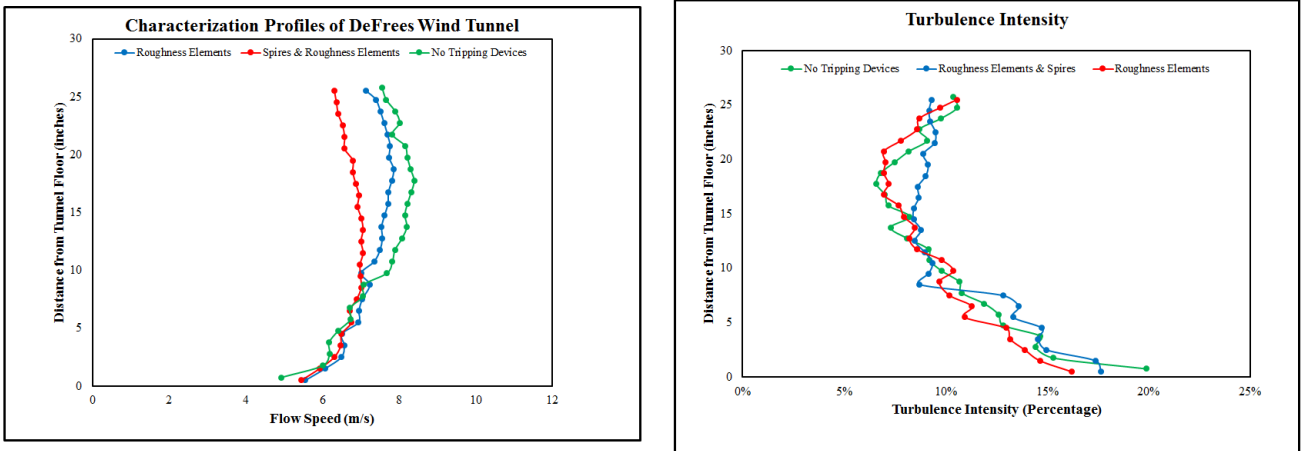


**Figure 8. Characterization profiles and turbulence intensity for the DeFress Wind Tunnel**

Because the spires are also meant to increase turbulence within the tunnel, we calculated the turbulence intensity for the three profiles to use for future testing. Fig. 8 has the plots of the three profiles and their respective turbulence intensity shown as a percentage. Fig. 8 also shows that the spires do generate an increase in turbulence intensity as well as shifting our boundary layer to a regime we desire. With all preliminary data and tests taken we were able to move forward to running tests with models of different geometries.

#### D. Experiments

Our experiments focus on how geometry affects wind flow so we performed tests on two different models. The first being a rectangular block with dimensions 11.75 inches high and 6 inches wide. The length was made to be almost the width of the tunnel since our tests are only meant to be a 2D plane section of the flow through the tunnel. The second model, was similar to the first only differing by its façade having a 30° slope normal to the wind flow. The test ran starting at a point 3.5 inches in front and 0.5 inches above of the model’s roof leading edge across a grid, spaced by half inch increments in both directions, ending at a point 3.5 inches behind and 11.5 inches above the roof’s trailing edge. All testing data was captured by Labview and then ran through a Matlab data processing script to produce usable results and plots.

## VI. Results

We will consider the two cases in order of increasing complexity. We first compare the rectangular block, meant to represent a standard building shape, to the free stream to note any improvement we gain by simply having a structure in the flow. We then move on to the case of the sloped block and compare it to both the free stream and the rectangular baseline design. In both cases, the velocity distribution is the main result, with secondary results such as available wind power and turbulence intensity providing important contextual information for the placement of small wind turbines.

### A. Rectangular Block

The results for the rectangular block are presented first.

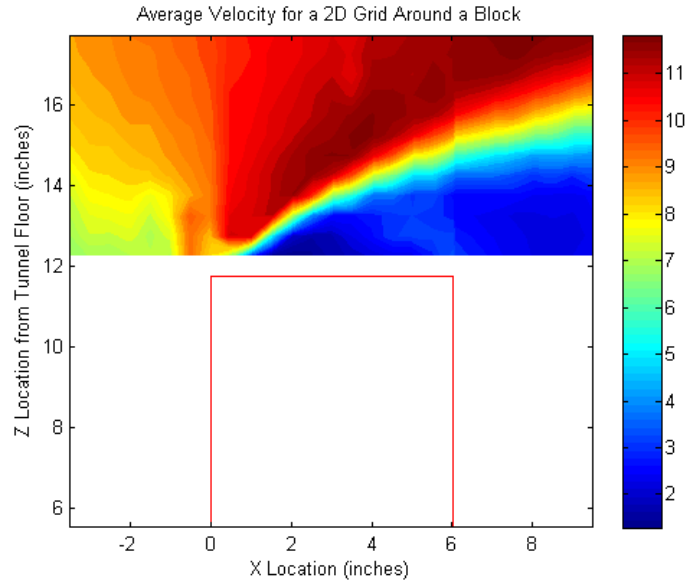


**Figure 9: Average Velocities at Points Around Rectangular Block in Flow with Mean Speed 8.19 m/s**

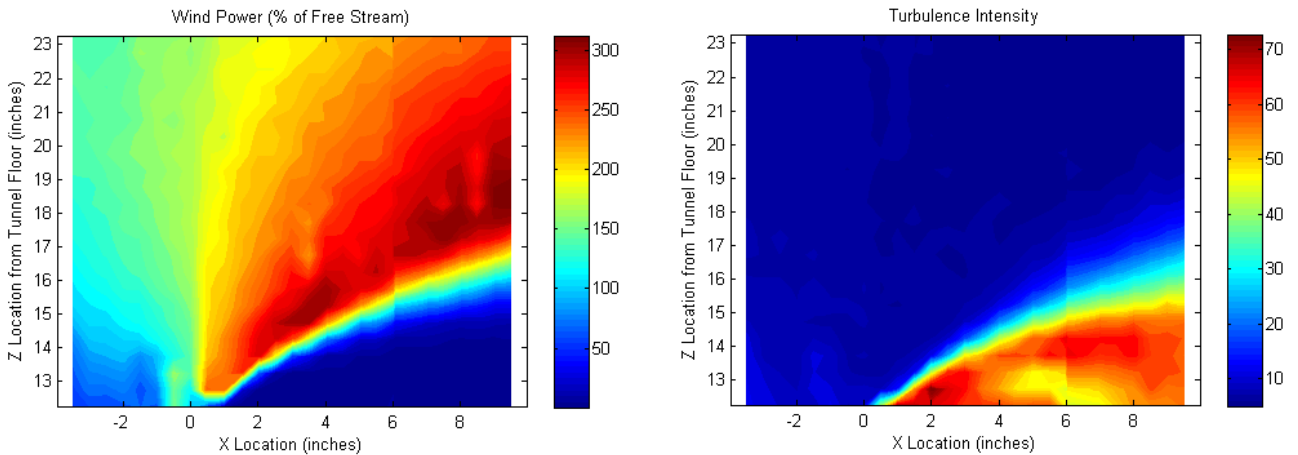


**Figure 10: Wind power at testing points relative to wind power in free stream , and turbulence intensity.**

As can be seen from the above plots, the rectangular structure is able to accelerate the flow to produce power that is over three times as large as that contained in the free stream. However, these velocities are only achieved in a region where it is probably unfeasible to mount a wind turbine (i.e. around 14m from the building top using our scale factor). Although we would likely be unable to take advantage of these large velocities, we still get a sizable increase in power if we place our hypothetical turbine closer to the leading edge, where heights of just 7.5m can lead to power increases of over 200%.

We observe as well that due to the bluff nature of the building structure, a sizable boundary layer develops off the leading edge. This boundary layer is characterized by low average wind speeds and high turbulence, which is exactly what we are trying to avoid. Thus, we rule out the rest of the rooftop for placement of the turbine. This is in line with our expectations since we would expect the no-slip condition to apply at the rooftop. That being said, it is worth noting that the turbulence intensity at the leading edge, provided we have broken out of the boundary layer, is small.

## B. Sloped Block

One of the main goals of this project is to find optimal building geometries for harvesting wind energy. We thus note that one of the major obstacles that presented itself in the rectangular block case was the thick boundary layer that is generated off the sharp corner at the leading edge of the rooftop in that model. One of the ways to get around this undesirable characteristic is to give the flow a more gradual adjustment to the obstacle. In our case, this was done by creating a building model whose façade slopes at an angle of 30 degrees to the horizontal.

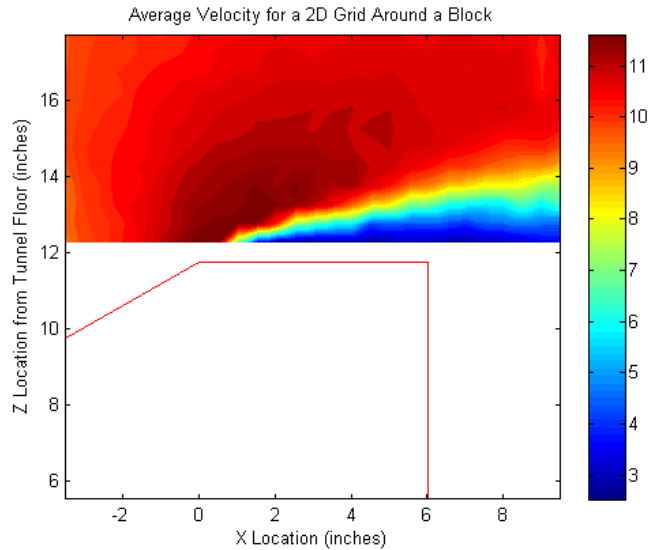


**Figure 11: Average Velocities at Points Around Sloped Block in Flow with Mean Speed 8.19 m/s**

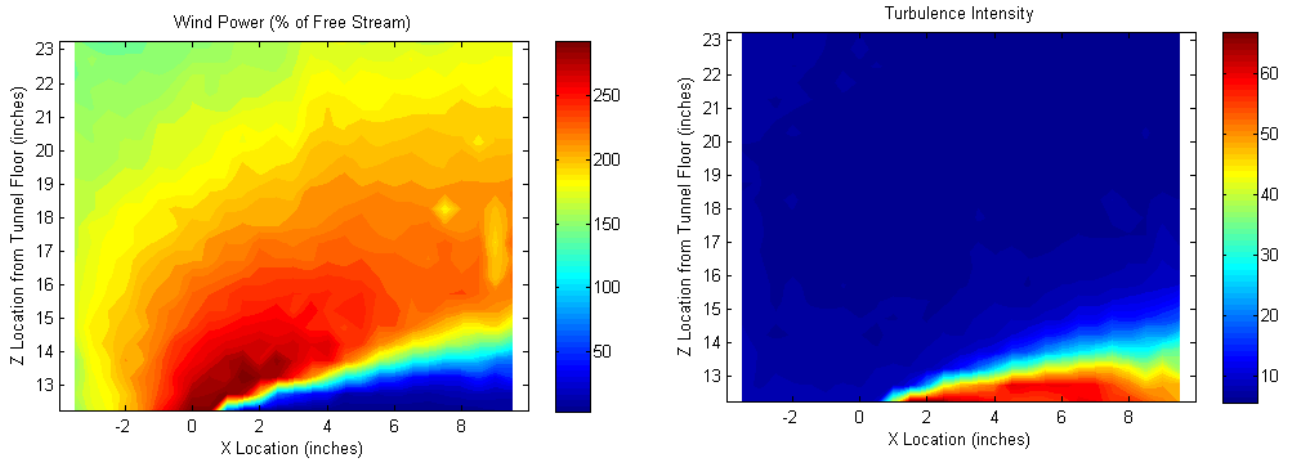


**Figure 12: Wind power at testing points relative to wind power in free stream, and turbulence intensity.**

The most striking characteristic of this new sloped model is the relative thinness and slower development of the boundary layer at the rooftop. A thin boundary layer means we have more options on the sorts of turbines or other wind-power solutions we can place at the leading edge. Furthermore, we see that we still retain most of the immense flow acceleration which was seen in the rectangular model. However, in this case, the flow acceleration is all concentrated around the leading edge, where there is also minimal turbulence.

## VII. Conclusion

Buildings account for a large portion of total electricity use across the United States. Finding clean, renewable ways to offset this energy on a per-building basis could be very beneficial to the country. As such experiments and simulations were designed to simulate the atmospheric boundary layer (where buildings reside) and investigate the resulting flow around models of varying dimensions and geometry. After configuring the roughness elements and spires to simulate free-stream flow conditions that are found near buildings, we tested two models: one with a “standard” rectangular façade, and one with a façade that sloped at an angle of 30 degrees relative to the horizontal. We found that both models accelerated the flow around the leading edge of their rooftop. This accelerated flow led to an maximum power potential of 3 and 2.5 times the free stream for the rectangular and sloped models respectively. However, we found that the sloped model produced a much thinner boundary layer and accelerated its flow near the leading edge which makes it much more suitable for placement of a small wind-turbine. We found that the maximum turbulence for both models was similar, but since the sloped model had a thinner boundary layer, the maximum turbulence in that case occurred much farther from the leading edge. We thus conclude that by altering the geometry of buildings we can significantly influence the flow in favor of wind power generation. Future experiments will expand on the optimization process and consider more exotic building shapes.

## VIII. Further Work

After this project was presented at the AIAA conference at Cornell on April 25<sup>th</sup>, further work was done in fine tuning the conditions in the tunnel. Since the original experimental set-up we used did not achieve an urban atmospheric boundary layer but rather one closer to rural conditions, we had make changes to the arrangement of tripping devices. The ultimate goal for the following tunnel characterizations was to achieve a “power-law” profile of the form

$$\frac{u}{u_r} = \left(\frac{z}{z_r}\right)^\alpha \quad (11)$$

where  $u_r$  is the reference velocity at the reference height  $z_r$  and  $\alpha$  is simply the coefficient that is derived by regressing the data. Specifically, we were trying to achieve a profile that had an  $\alpha$  value in the range that published results state correspond with urban areas. According to Counihan<sup>12</sup>, an  $\alpha$  value of at least 0.21 and up to 0.4 is necessary in order to properly simulate urban atmospheric boundary conditions in a wind tunnel.

To do this, we first needed to increase the amount of roughness elements, now at 12 meters long, in the fetch. Next, we reduced the initial flow blockage by reducing the number of spires. Then, we introduced a new tripping device in the form of a rectangular barrier stretching the width of the tunnel. After introducing these changes, we ran a number of profiles to try to match the published data by modifying the barrier height and number of spires.

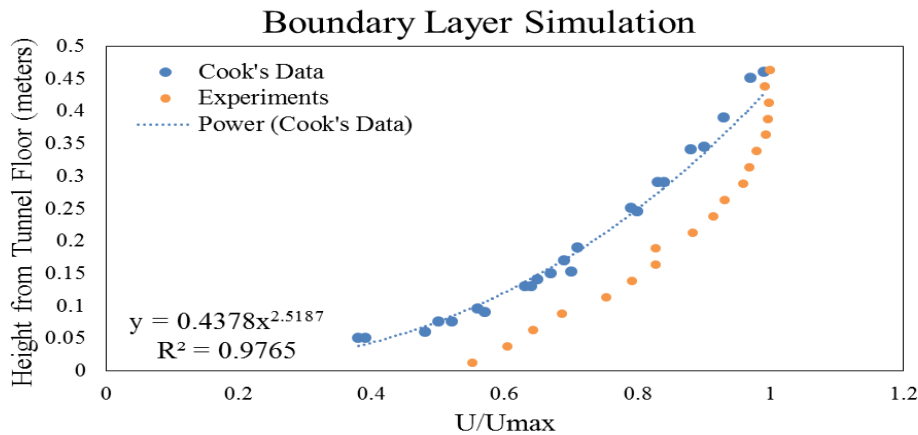
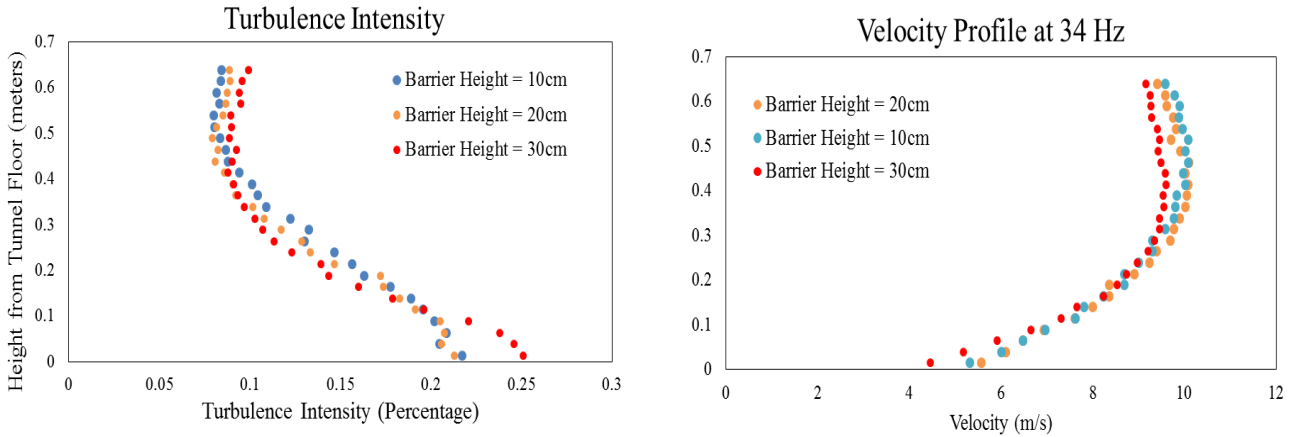


Figure 13: First Characterization with Increased Amount of Roughness Elements

As can be seen from the above plot, our initial attempt at achieving the prescribed  $\alpha$  value was not very successful. The experimental data presented for comparison in this plot had an  $\alpha$  value of 0.39, which was not at all

in agreement with our result. Thus, the decision was made to add another tripping device into the tunnel, this time in the form of a rectangular “splitter-plate” between the spires and the beginning of the roughness elements. The effect of the varying dimensions of this plate can be seen below. At this point, it should be mentioned that all tests were done at a free stream velocity of 10 m/s in order to force consistency.



**Figure 12 (left) and 13 (right): Effect of Increasing Barrier Height on Turbulence Intensity and Velocity**

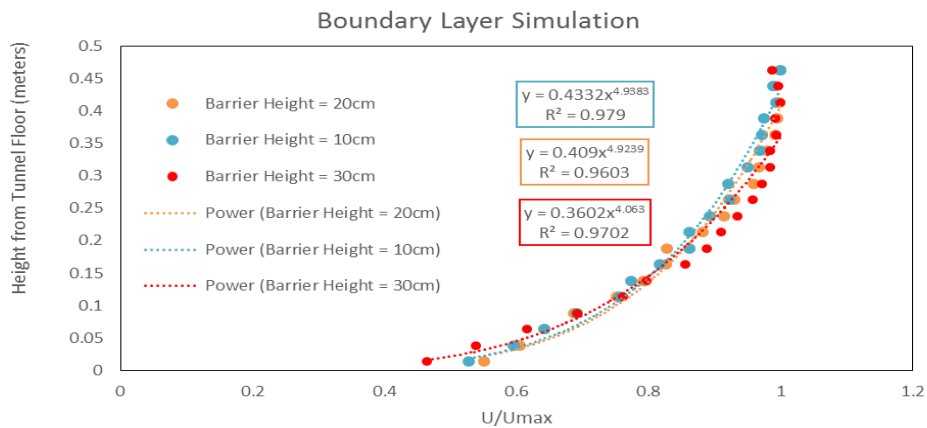


**Figure 14: Power Law Regressions for Increasing Barrier Height**

**Fig. 14** shows the the power-law regressions of the data with increasing barrier height (though it should be noted that the exponents presented in the figure are the inverse of the  $\alpha$  presented in equation (11)). We see that the the coefficient barely varied between the 10cm and 20cm barrier heights, increasing only to 0.203 from 0.202, still short of the 0.21 goal. However, at the 30cm barrier height, we finally break through into the desired range, achieving an  $\alpha$  of 0.246. Recently, we ran a profile that keeps all parameters constant as presented in the 30cm barrier case, but increases the length of the roughness elements once more. This was to see if we could fine tune the profile even further and achieve a higher  $\alpha$ .

In addition to attempting to simulate the correct profile, we also wanted to make sure the tunnel produced homogenous data along its width. Although unimportant for 2D tests, any differences along the width of the tunnel would produce major errors in a 3D test.

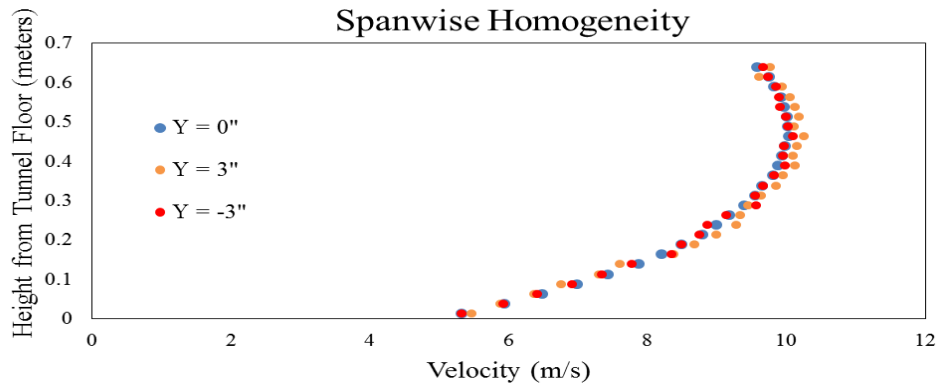


**Figure 15: Test of Spanwise Velocity Homogeneity**

From **Fig. 15**, we can see that the profiles 3 in. on either side of the centerline (where all the other profiles and 2D tests were performed) are virtually identical to the one in the middle. Thus, we can rest assured that our upcoming 3D tests will not suffer from inconsistent conditions in the tunnel.

### Acknowledgments

The authors would like to acknowledge Prof. Ephraim Garcia, Malika Grayson and Dr. Michael Shafer for their guidance and support throughout this project. We thank Justin Yeh and Peter Ericksen for their help in running the experiments. We would also like to thank Cornell University for providing us with the resources and facilities to conduct our research, and Prof. Edwin Cowen for letting us use the DeFrees Laboratory wind tunnel for the experiments.

### References

- <sup>1</sup>Sharpe, T., Proven, G., "Crossflex: Concept and early development of a true building integrated wind turbine," *Energy and Buildings*, Volume 42, Issue 12, December 2010, pp. 2365-2375.
- <sup>2</sup>"20% Wind Energy by 2030" *US Department of Energy*. Energy efficiency and renewable energy. July 2008.
- <sup>3</sup>Heath, M., Walshe, J.D., "Estimating the Potential Yield of Small Building-mounted Wind Turbines," *Wind Energ.* 2007; 10:271–287 Published online 8 March 2007 in Wiley Interscience (www.interscience.wiley.com) DOI: 10.1002/we.222.
- <sup>4</sup>Glass, A., and Levermore, G., "Micro wind turbine performance under real weather conditions in urban environment," *Building Serv. Eng. Res. Technol.* 32,3 (2011) pp. 245–262.
- <sup>5</sup>Dannecker, R., and Grant, A.D., "Investigations of a Building-Integrated Ducted Wind Turbine Module," *Wind Energ.* 2002; 5:53–71 (DOI: 10.1002/we.60).
- <sup>6</sup>"Annual Energy Review 2011" *U.S. Energy Information Administration*. 2011.
- <sup>7</sup>Manwell, J.F., McGowan, J.G., Rogers, A.L., *Wind Energy Explained*, 2<sup>nd</sup> ed., Wiley, England, 2009, Chaps. 1, 2.
- <sup>8</sup>"55M System with a 55M10 CTA Standard Bridge," *DISA Technical Manual*.
- <sup>9</sup>Irwin, H. P. A. H. (1980). "The design of spires for wind simulation" *Journal of Wind Engineering and Industrial Aerodynamics*.
- <sup>10</sup>Abrahamsen, Ida S., "Wind Tunnel Model Testing of Offshore Platforms" *Norwegian University of Science and Technology*, June 2012
- <sup>11</sup>Gartshore, I. S., "Roughness Element Geometry Required for Wind Tunnel Simulations of the Atmospheric Wind", *The University of British Columbia*, September 1977
- <sup>12</sup>Counihan, J. "Simulation of an Adiabatic Urban Boundary Layer in a Wind Tunnel." *Atmospheric Environment* (1967) 7.7 (1973): 673-89. Print.